Appl. Phys. A 81, 1627–1632 (2005)
DOI: 10.1007/s00339-005-3326-x

Applied Physics A
Materials Science & Processing

I.H. CHOWDHURY[1]
A.Q. WU[1]
X. XU[1,✉]
A.M. WEINER[2]

Ultra-fast laser absorption and ablation dynamics in wide-band-gap dielectrics

[1] School of Mechanical Engineering, Purdue University, West Lafayette, IN 47907, USA
[2] School of Electrical and Computer Engineering, Purdue University, West Lafayette, IN 47907, USA

Received: 30 March 2005 / Accepted: 27 June 2005
Published online: 2 August 2005 •

ABSTRACT The highly nonlinear laser–matter interaction conditions produced by high-intensity amplified ultra-fast laser pulses have proven to be beneficial in the processing of normally transparent wide-band-gap dielectric materials. This article presents experimental studies of the ultra-fast laser absorption process in three wide-band-gap dielectrics: fused silica, calcium fluoride, and sapphire. Time-resolved measurements of the probe transmissivity and reflectivity show both the formation of dense free-electron plasma at the surface due to nonlinear absorption of the laser pulses and rapid structural damage on the order of a few picoseconds. Pump–probe data with intense pump and probe pulses was also correlated to atomic force microscopy measurements of the ablated volume. It was observed that the material removal peaked near zero delay between the pulses and decreased within a temporal separation of about 1 ps.

PACS 52.38.Mf; 78.47.+p; 79.20.Ds

1 Introduction

Ultra-fast lasers are a unique tool for machining a diverse range of materials. In particular, the highly nonlinear laser–matter interaction conditions produced by ultra-fast pulses are conducive to the processing of hard-to-machine materials such as ceramics and wide-band-gap dielectrics. Wide-band-gap dielectrics such as fused silica are normally transparent to visible and near-infrared light as the photon energy is insufficient to excite an electron from the valence to the conduction band by linear absorption. However, the extremely high intensities created by amplified ultra-fast laser pulses cause nonlinear photoionization effects which lead to significant absorption of the photons. This topic has received considerable attention in recent years and several reviews of the existing literature are available [1, 2]. Briefly, an electron in the valence band can absorb several visible or near-infrared photons and gain enough energy to cross the band gap. This process is referred to as multiphoton ionization. Another nonlinear photoionization process that becomes important at high electric field magnitudes is tunneling photoionization, where the strong electric field suppresses the Coulomb barrier and allows the electron to tunnel through. The free electrons created by nonlinear photoionization can then absorb more energy from the laser pulse by inverse bremsstrahlung. If the energy of the free carriers becomes high enough, they can also promote an electron from the valence to the conduction band by impact ionization leading to an avalanche process.

The free-electron plasma created in wide-band-gap dielectrics by the nonlinear absorption of ultra-fast laser pulses has been observed in both time-resolved reflectivity [3] and shadowgraph imaging experiments [4]. Vu et al. [3] observed an increase in the reflectivity of fused quartz irradiated with 100-fs pulses that lasted for about 10 ps. Simultaneous measurements of the Doppler shift of a probe reflected from the back side of the sample revealed that the ionization front moved into the sample with a maximum velocity of 1.8×10^5 m/s. Similar high-reflectivity signals of the order of 60% were observed in several different dielectric samples by von der Linde and Schüler [5], who also noted that the threshold intensity for plasma formation was close to 10^{13} W/cm^2. Spectral interferometry studies have revealed that the free carriers created by the femtosecond pump pulse can be captured very rapidly in some materials like fused silica due to the formation of self-trapped excitons (STEs) [6]. A trapping time of 150 fs was measured for fused silica while the carriers remained free in sapphire for 100 ps. Transient absorption experiments in calcium fluoride revealed a similar effect with a STE formation time of 690 fs [7].

Time-resolved measurements of plasma emission under double-pulse irradiation in fused silica and its correlation to the optical breakdown threshold (OBT) have also been reported [8]. It was observed that the OBT for the second pulse gradually increased until a delay of 200 fs between the pulses and then stayed almost constant and finally recovered slowly to the value for single-pulse OBT in a period of about 2.5 ns. A simple rate-equation model with an exponential decay term for the free-electron distribution could not explain the experimental results. However, it was pointed out later [9] that the results could be explained in terms of the STE effect mentioned above. Moreover, the STEs can act as suitable sites for the absorption of the subsequent pulse as the electron in the e – h pair is more weakly bound than the valence-band electrons. The STE itself recombines over a time scale of nanoseconds, which can explain the observed recovery behavior of the OBT for the second laser pulse. Thus, a combination of absorption in the free carriers in the first few hundred femtoseconds and in the STE in the subsequent period was held

✉ Fax: +1-765-494-0539, E-mail: xxu@ecn.purdue.edu

responsible for the observed OBT dynamics in fused silica. Machining of fused silica and other dielectric samples with double- and triple-pulse sequences synthesized using a pulse shaper has also been reported [10]. A significant difference in the OBT under multiple-pulse irradiation of fused silica and sapphire was observed. The OBT changed rapidly within 1 ps for fused silica, in accord with the results from the previous studies, while the OBT for sapphire did not change much over this time period. This is attributed to the fact that fused silica has a fast trapping of free electrons due to the STE effect while in sapphire the excited carriers can remain free for much longer periods. It was also observed that increasing the separation from 0.3 ps to 1 ps for a triple-pulse sequence led to a decrease in the amount of material ablated for the case of fused silica but not for sapphire.

Some experiments have been carried out using pulse trains of high repetition rate and interesting machining effects have been reported. Herman et al. [11] used a train of 430 pulses of 1.2-ps duration each for machining fused-silica samples and found that the surface microcracking or swelling that occurred with single-pulse machining could be eliminated. It was assumed that the heating effects associated with the high repetition rate may have improved the ductility of the surrounding glass. A four-pulse sequence was also used to machine various materials including glass and significant changes in the machining characteristics could be observed [12]. Some amount of enhancement in machining quality due to the use of ultrafast pulse trains generated by pulse shapers has also been reported [10]. As such, it is seen that machining with a pulse train with a repetition rate of the order of GHz to THz instead of a single pulse repeated at the amplifier rate of a few kHz could possibly offer certain advantages, combining the positive aspects of both short- and long-pulse interactions. However, the fundamental reasons why pulse trains could offer advantages to material-removal applications are still not very well understood.

As discussed previously, the interaction of ultra-fast laser pulses with wide-band-gap dielectrics involves the absorption of photons by the valence electrons and subsequent coupling of the energy to the lattice. The absorption itself is quite a complex phenomenon as the free-electron plasma generated by the initial part of the pulse can either absorb the later part more efficiently or act as a plasma mirror and reflect most of the energy [13, 14]. For material-processing applications, it is desirable that most of the energy of the pulse be absorbed in the sample. Another question that relates to the lifetime of the photoexcited carriers is: how long do the carriers remain free before they are captured as STEs or in defect states? Also, the creation of STEs can affect the absorption of the subsequent pulses as they represent energy levels within the band gap that can be excited much more easily. All these issues would affect how well the later pulses in a train are absorbed in the material. This article aims to resolve some of these questions by conducting pump–probe experiments on different dielectric samples to identify the absorption characteristics and also relate these to the ablation process. Sect. 2 describes the experimental setup while the results of single-pulse and time-resolved pump–probe experiments are presented in Sect. 3.

2 Experimental setup

The experimental setup is a typical pump–probe arrangement with orthogonal polarization of the two pulses as shown in Fig. 1. The input is a 90-fs FWHM (full width at half maximum) pulse centered at 800 nm emitted by a Ti:sapphire regenerative amplifier. Single pulses are selected from the 1-kHz pulse train with an electromechanical shutter. A half-wave plate (HWP) placed in the probe-beam path rotates the probe polarization from horizontal to vertical. The power of the pump and probe beams is controlled by using neutral-density (ND) filters and half-wave-plate/polarizer combinations (not shown in the diagram). The pump and probe beams are focused on the sample with a long-working-distance Mitutoyo objective (10×, 0.28 NA). The sample itself is mounted on a motorized stage so that it can be moved perpendicular to the beam between pulses, allowing a fresh surface to be exposed to each laser pulse. The transmitted part of the beam is collected with another objective (50×, 0.5 NA) and sent to the second photodetector (PD2). The collecting objective has a much higher NA than the focusing objective in order to ensure that all the transmitted light is collected. The part of the beam that is reflected normally is collected by the focusing objective and sent back towards the third photodetector (PD3). Appropriate polarizers (P) and 800-nm band-pass filters (F) were placed in front of the photodiodes to block the pump beam and plasma light. The CCD camera along with a white-light source (not shown in the diagram) images the surface of the sample using the focusing objective. This helps in controlling the location of the sample surface with respect to the focal position to ensure repeatability during the experiments. Moreover, the imaging setup can also be used to image the air breakdown at very high incident energies. This helps to

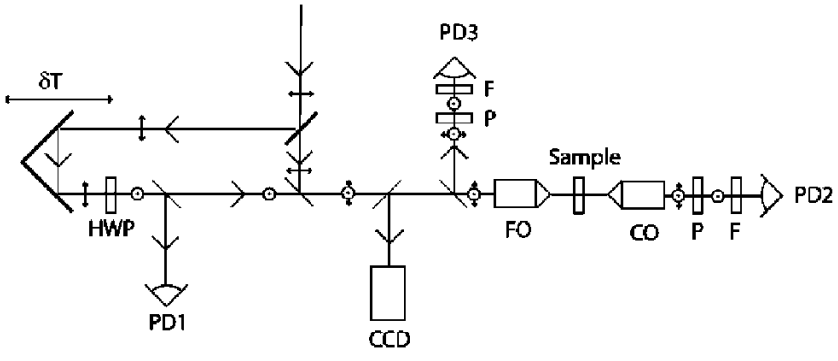

FIGURE 1 Schematic layout of pump–probe setup. HWP: half-wave plate, PD: Si photodetector, CCD: CCD camera, FO: focusing objective, CO: collecting objective, P: polarizer, F: 800-nm band-pass filter

locate the focal position at the imaging plane and hence also the position of the sample surface with respect to the focus. The position of the focus is not expected to vary with the incident energy, since the critical power for self-focusing in air is quite high (1.7 GW) [15] compared to typical peak powers of about 10 MW in our experiments. The pump–probe setup can be easily used for single-pulse measurements by blocking the pump beam and using the vertically polarized probe beam only. The processed samples are analyzed with an atomic force microscope (AFM) to measure the ablated volume.

3 Results and discussion

3.1 *Single-pulse measurements*

Following the discussion in Sect. 1, it is expected that, as the intensity of the incident pulse is increased, the transmissivity should drop and the reflectivity should rise since the free-electron plasma in the conduction band created by nonlinear absorption of the initial part of the pulse absorbs and reflects the later part of the pulse. As the intensity increases, more electrons are photoexcited to the conduction band and the free electron plasma density increases. Mathematically, the idea can be expressed in terms of the plasma-frequency concept based on the Drude model [16], which states that the reflectivity increases sharply when the plasma frequency becomes equal to the laser frequency.

The experimentally obtained values of single-pulse transmissivity and reflectivity as a function of incident laser fluence are shown in Fig. 2. Three different dielectric samples were considered: calcium fluoride (CaF_2, 2-mm thick, Alfa Aesar), fused silica (SiO_2, 1-mm thick, Corning 7980), and sapphire (Al_2O_3, 2-mm thick, Edmund Optics). The intensity values quoted here are based on a beam spot size of 4 μm (measured by a knife-edge technique) and a pulse width of 90 fs FWHM (measured by a single-shot autocorrelator and by two-photon absorption autocorrelation in a GaP photodiode). The data is calibrated to obtain absolute values for transmissivity and reflectivity by using the fact that at the lowest intensities the free-electron density will be negligible and hence the reflectivity and transmissivity values can be calculated from the normal refractive-index values at $\lambda = 800$ nm. As predicted by theory, the transmissivity drops and the reflectivity rises for all the three wide-band-gap dielectric samples as the incident intensity is increased. It is seen that the transmissivity drop is the smallest for CaF_2 and very similar for SiO_2 and Al_2O_3. This phenomenon is partly related to the values of the band gaps of the three materials: 12 eV for CaF_2 [7] and 9 eV for SiO_2 [17] and Al_2O_3 [18]. As the absorption is by nonlinear photoionization, the value of the band gap will determine how easily the incident photons will be absorbed. A larger band gap could lead to less absorption and hence higher transmissivity. However, at the high intensities considered here, the effects of free-electron absorption are expected to dominate the transmissivity, as the intensity is high enough to create the initial seed plasma regardless of the band-gap value.

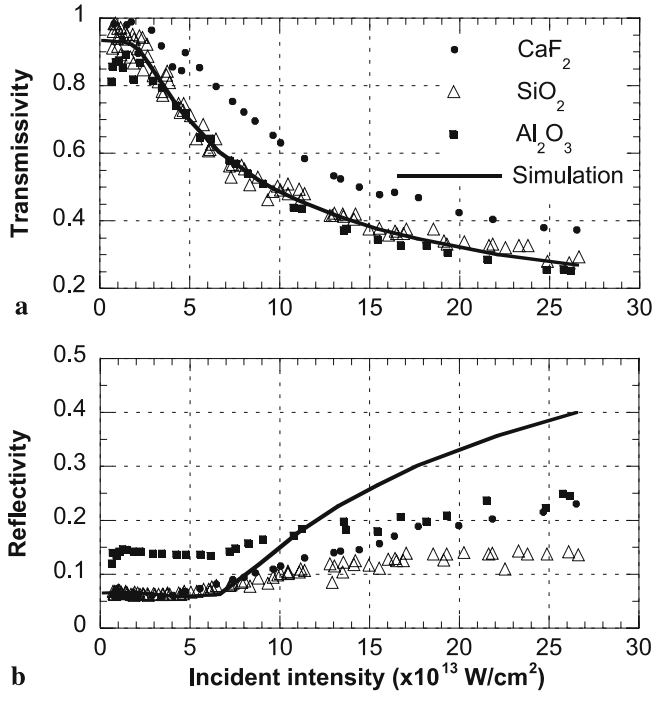

FIGURE 2 (**a**) Transmissivity and (**b**) reflectivity of a single 90-fs, 800-nm pulse as a function of incident intensity in various wide-band-gap dielectric samples

In Fig. 2, the solid line for SiO_2 is obtained from a numerical model that simulates the propagation of ultra-fast laser pulses inside fused silica using the 2 (spatial) + 1 (temporal)-dimensional propagation equation given below:

$$\frac{\partial}{\partial z}\psi = \frac{\mathrm{i}}{2k}\nabla_\mathrm{t}^2\psi - \frac{W_\mathrm{PI}\,U}{nc_0\varepsilon_0|\psi|^2}\psi - \mathrm{i}\,\frac{k''}{2}\frac{\partial^2\psi}{\partial t'^2} + \mathrm{i}k_0 n_2\frac{nc_0\varepsilon_0}{2}|\psi|^2\psi - \frac{\sigma}{2}\varrho\psi - \mathrm{i}\frac{\sigma}{2}\,\omega\,\tau\,\varrho\,\psi. \quad (1)$$

Here, $\psi(r, z, t)$ is the envelope function of the electric field, ∇_t^2 the Laplacian operator in the transverse plane, W_PI the photoionization rate obtained from the Keldysh theory [19], k'' the group velocity dispersion coefficient, $t' = t - z/v_\mathrm{g}$ the retarded time, k_0 the laser wavenumber in vacuum, ε the complex relative dielectric constant of excited fused silica, and $n = \mathrm{Re}\sqrt{\varepsilon}$ the corresponding refractive index. The first term on the right-hand side in (1) stands for laser diffraction in the transverse plane, the second term accounts for absorption due to nonlinear photoionization, and the third term represents the group-velocity dispersion. The last three terms on the right-hand side account for self-focusing related to the Kerr effect, free-electron absorption, and laser defocusing due to the free electrons, respectively. A more detailed description of the model can be found in [20]. The evolution of the free-electron density ρ in fused silica is described with the following rate equation:

$$\frac{\mathrm{d}\rho}{\mathrm{d}t} = (W_\mathrm{PI} + \beta I\rho)\left(1 - \frac{\rho}{\rho_\mathrm{max}}\right) - \frac{\rho}{\tau_\mathrm{s}}. \quad (2)$$

Here, β is the avalanche ionization coefficient and τ_s the electron trapping time. Together, (1) and (2) are solved numerically to predict the propagation of femtosecond pulses in bulk fused silica, taking into account both reflection at the air–solid interface and the absorption mechanisms in the bulk that contribute to the final transmissivity value.

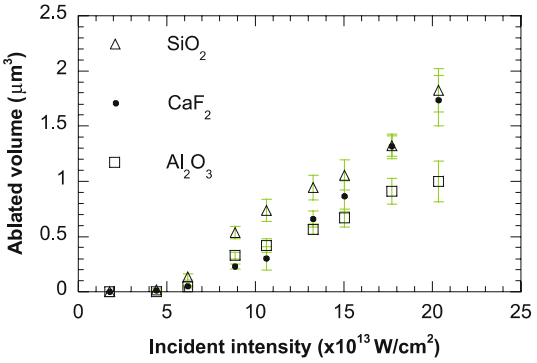

FIGURE 3 Ablated volume measured with AFM as a function of incident intensity for various wide-band-gap dielectrics

It is seen from Fig. 2 that the transmissivity fit is quite good but the reflectivity prediction is much higher than the experimentally observed values except at the lowest intensities. The reason for this is that as the intensity increases, there is a considerable amount of scattering of the pulse in all directions. This was observed by using an infrared viewer fitted with an 800-nm band-pass filter. As the model does not provide for scattering, and the experiment picks up only the normally reflected part of the light, the reflectivity data does not match the model predictions. Similar experiments have been reported by other groups [13, 14]. In these cases, the experimentally observed reflectivity values were higher than the ones shown here and matched model predictions quite well. The main reason for this difference is due to the focusing conditions. The experiments in the two references mentioned above used very slow focusing lenses ($f \sim 1000$ mm), while this study uses a very tight focusing objective. As a result, the free-electron plasma created in this experiment is confined to a very small volume ($\sim$ 4-μm diameter). This is expected to create a much more uneven and unstable plasma that causes scattering in all directions instead of specular reflection.

The volume of ablated material for a single pulse at different incident intensities was measured using an atomic force microscope (AFM) and the data is presented in Fig. 3. Each data point is averaged over five measurements and the error bars represent the standard deviation. The larger band gap and corresponding higher transmissivity of CaF_2, as seen in Fig. 2a, would imply lower absorption in this dielectric and hence less ablation. However, it is noticed that Al_2O_3 has the smallest ablated volume. This phenomenon can be explained in terms of the enthalpy of fusion of the three materials, which is a measure of the bond strengths. Al_2O_3 has the highest enthalpy at 111.1 kJ/mol followed by CaF_2 (29.71 kJ/mol) and SiO_2 (8.51 kJ/mol) [21]. Because of this, it is to be expected that even if there is less absorption in CaF_2, there will be greater material removal because it can be damaged more easily. The two other materials also show the expected trend in ablated volume corresponding to their respective enthalpies, although there is some overlap between CaF_2 and Al_2O_3 at the lower intensities that is within the margin of error.

3.2 *Time-resolved measurements*

As discussed in the introduction, the primary goal of this work is to assess the effect of material removal with a pulse train instead of a single pulse. To this end, pump–probe experiments were carried out to measure the effect of the free-electron plasma created by the pump pulse on the probe transmissivity and reflectivity. A weak, vertically polarized probe pulse at an intensity level of 0.88×10^{13} W/cm^2 was used. The pump pulse was horizontally polarized and four different intensities were considered: 1.77×10^{13}, 4.42×10^{13}, 7.96×10^{13}, and 10.61×10^{13} W/cm^2. The first value is much below the damage threshold. The second is very near the damage threshold as seen from Fig. 3 and the last two are above the damage threshold. The pump–probe data for the three dielectrics is shown in Fig. 4, 5, and 6 (negative delay corresponds to the probe pulse arriving before the pump). Each point in the plots corresponds to an average over five data points. The standard deviation is calculated to be about 10%–15% for the transmissivity values and about 20%–30% for the reflectivity values. The error bars corresponding to these values are not shown in the figure for clarity.

It is observed from the figures that all three dielectrics show very similar temporal behavior, in contrast to previous studies that have reported that the free carriers in these three dielectrics have very different lifetimes ranging from 150 fs in SiO_2 to 100 ps in Al_2O_3 [6, 7]. There is no appreciable change at the lowest intensity as the free-electron density excited by the pump is still quite low. As the pump intensity is increased, there is a sharp drop in transmissivity around $t = 0$ and then a slow increase on the order of 10–100 ps. The reflectivity shows a sharp rise at zero delay and then starts to decay after 2–3 ps, finally reaching a value much below the initial reflectivity after about 10 ps. The increase in reflectivity is due to the creation of free-electron plasma, as was also observed in the single-pulse experiments. As the pump intensity is increased, there is a corresponding increase in the free-electron density

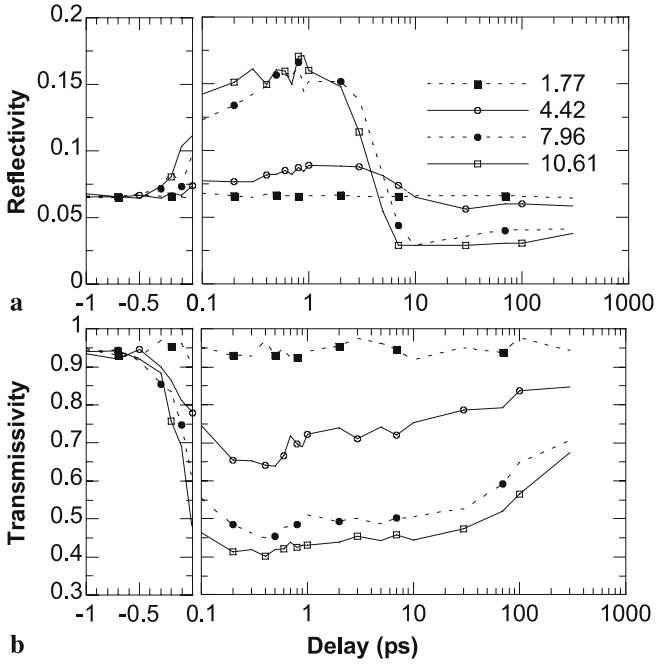

FIGURE 4 Time-resolved (**a**) reflectivity and (**b**) transmissivity of a 0.88×10^{13}-W/cm^2 probe at different values of pump intensity for fused silica

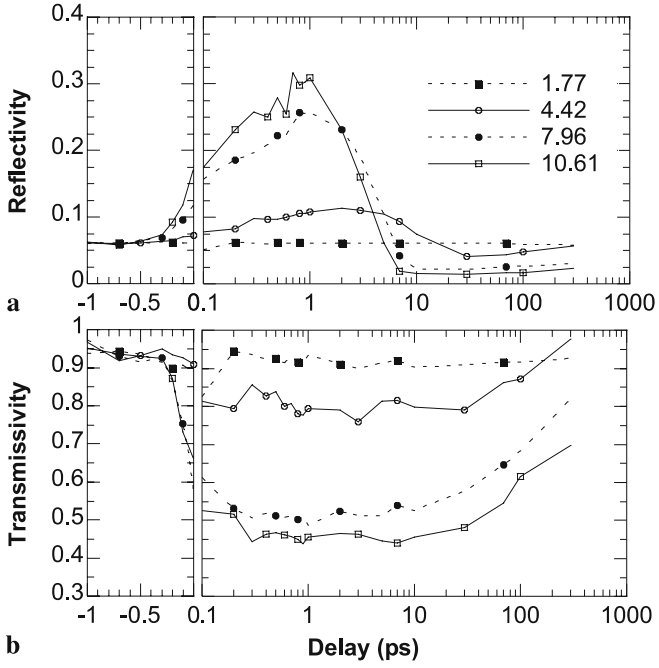

FIGURE 5 Time-resolved (**a**) reflectivity and (**b**) transmissivity of a 0.88×10^{13}-W/cm^2 probe at different values of pump intensity for calcium fluoride

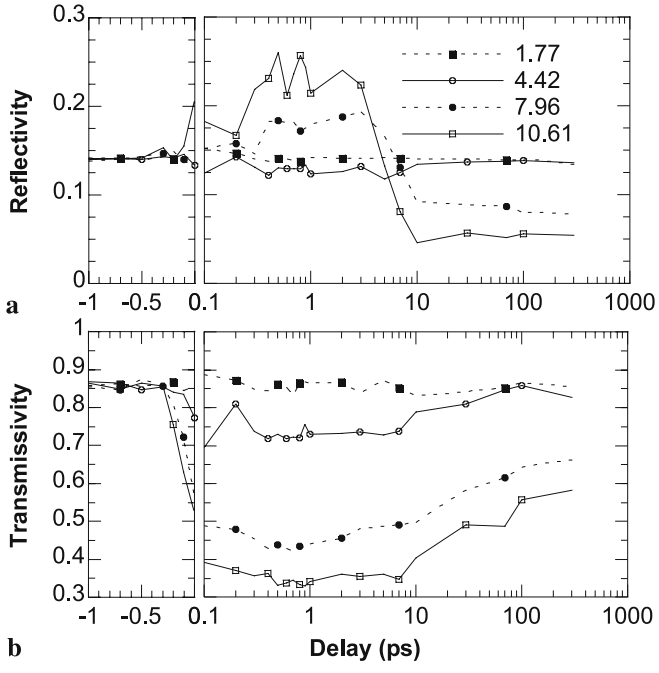

FIGURE 6 Time-resolved (**a**) reflectivity and (**b**) transmissivity of a 0.88×10^{13}-W/cm^2 probe at different values of pump intensity for sapphire

and hence the reflectivity of the probe. The difference in the time scales of the change in transmissivity and reflectivity is due to the fact that reflectivity is a function of the surface condition while transmissivity is more of a volume phenomenon. The sharp decrease in reflectivity after 2–3 ps is due to rapid structural damage at the surface of the sample which leads to scattering of the probe pulse, thus attenuating the reflectivity signal. However, the transmissivity depends on the propagation of the probe through the free-electron plasma in the bulk of the sample that lasts longer. Hence the slower dynamics in the transmissivity signal. We would like to emphasize here that the presence of scattering at the air–solid interface implies that a complete energy balance between the incident, reflected, and transmitted light measurements cannot be obtained in the present setup. What is measured is the specular reflection and transmission in the forward direction only.

On comparing the reflectivity curves for Al_2O_3 in Fig. 6 with the previous figures, it is observed that they are slightly different. The first difference is that a higher reflectivity (and correspondingly lower transmissivity) is observed at negative delays when the probe pulse sees the undisturbed material. This is attributed to the fact that, under normal conditions, Al_2O_3 has a higher refractive index than the other two materials, which contributes to the higher reflectivity. Also, it is seen that there is no change in the reflectivity signal at the second intensity level of 4.42×10^{13} W/cm^2 although there is a slight drop in transmissivity. This could be related to the fact that Al_2O_3 has a higher damage threshold (due to higher enthalpy of fusion) that was observed and discussed in the single-pulse experiments shown in Fig. 3 above. However, due to absorption in the bulk plasma, a drop in transmissivity can still be observed at this intensity level. At the two highest intensity levels, a rise in reflectivity and a drop in transmissivity are clearly observed, signifying that a dense free-electron plasma is formed at the surface. This behavior is similar to the case of the other two materials.

The presence of melting and resolidification during femtosecond laser processing of fused silica has been reported [22] and also melt-induced amorphization and crystallization in quartz and fused-silica samples [23]. However, the materials under investigation here are not expected to show a huge increase in reflectivity when they liquefy. For instance, experiments have shown that the change in reflectivity of sapphire on melting is quite small, as the extinction coefficient is of the order of 10^{-4} [24, 25]. Therefore, the reflectivity increase that we observe must be due to the photoexcitation of electrons from the valence to the conduction band. This could also have the effect of breaking the bonds between the atoms, leading to catastrophic sample damage that leads to the sharp decrease in the reflectivity signal seen in our experiments. Also, time-resolved measurements of the scattering of a probe pulse from fused silica show that the scattering signal rises after a delay of about 3 ps, which matches exactly with the onset of decay in our reflectivity signal [26]. However, the thermal effect in ablation can also play a role. The exact mechanism of surface damage needs further investigation.

In order to study the effect of time-dependent transmission and reflection on laser ablation, experiments were also conducted using two pulses with variable temporal separation, where both the pulses have equal intensities of 10.61×10^{13} W/cm^2. Figure 7 shows the ablation volume vs. temporal separation. The values for the transmissivity and reflectivity of the probe pulse are also plotted alongside. The ablated volume shows a maximum near zero delay in all three cases. In general, if the data is compared with the single-pulse ablation results shown in Fig. 3, it is observed that the ablated volume is slightly larger than that for a single pulse at an intensity of 10.61×10^{13} W/cm^2 for the longest delays and then slowly increases to a value near zero delay that is compara-

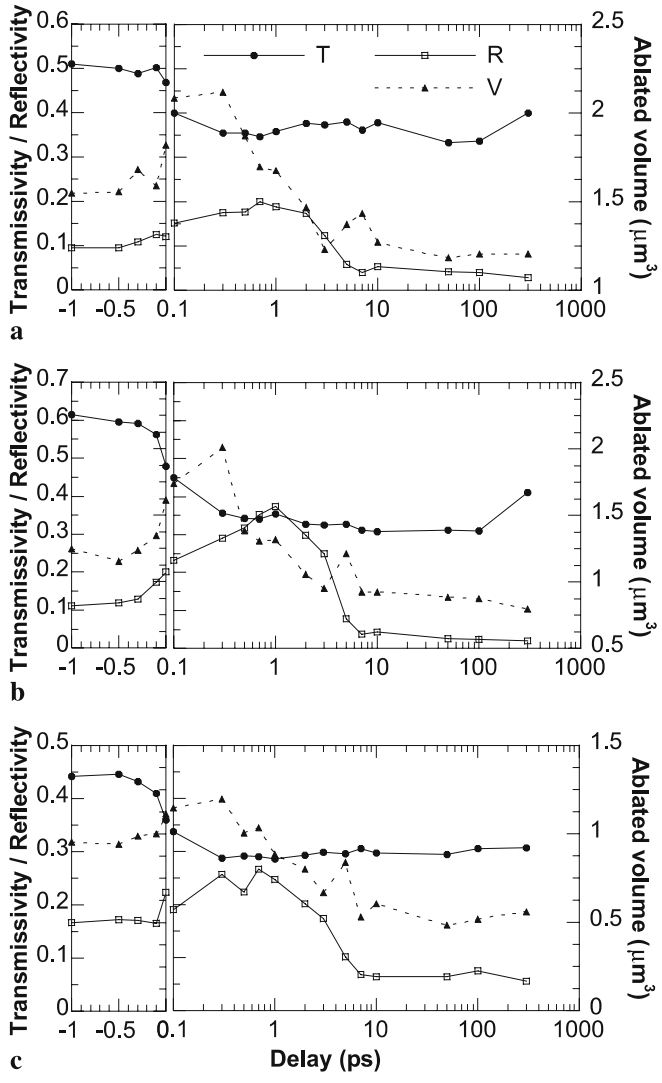

FIGURE 7 Time-resolved measurements of transmissivity, reflectivity, and ablated volume for the case where both pump and probe pulses have equal intensity of 10.61×10^{13} W/cm^2 in (**a**) fused silica, (**b**) calcium fluoride, and (**c**) sapphire. T: transmissivity, R: reflectivity, V: ablated volume

ble to that of a single pulse with double the intensity (within the margin of error). The decrease in ablated volume with increasing temporal separation is related to the interaction of the second pulse with the free-electron plasma created by the first pulse. On one hand, the free electrons can lead to enhanced absorption of the second pulse by inverse bremsstrahlung while, on the other hand, the reflectivity increase predicted by the Drude model can shield the second pulse from entering the sample. From our experimental results, it is seen that the second effect is dominant. Also, when the delay is longer than a few picoseconds, the surface structural damage will lead to scattering of the second pulse.

4 Conclusion

We have conducted single-pulse and pump–probe measurements of transmissivity and reflectivity for the fundamental 800-nm-wavelength pulses of an amplified ultra-fast Ti:sapphire laser in various wide-band-gap dielectric materials. The single-pulse data follow the expected trends of decrease in transmissivity and increase in reflectivity consistent with the creation of a free-electron plasma by nonlinear absorption of the initial part of the pulse that absorbs and reflects the later part. In the time-resolved pump–probe experiments, it was observed that the three dielectric materials considered in this study – SiO_2, CaF_2, and Al_2O_3 – showed very similar temporal behavior in spite of the fact that they have been reported to possess widely different free carrier trapping times. The strong reflectivity signal, corresponding to reflection by the dense free-electron plasma, was observed to decrease rapidly after 2–3 ps, which is attributed to rapid structural damage at the surface. Double-pulse ablation showed a maximum in ablated volume at zero delay and a rapid decrease with increasing temporal separation due to plasma screening by the free electrons created by the first pulse in the sequence.

ACKNOWLEDGEMENTS Support for this work by the National Science Foundation and the Indiana 21st Century Research and Development Fund is gratefully acknowledged.

REFERENCES

1 C.B. Schaffer, A. Brodeur, E. Mazur: Meas. Sci. Technol. **12**, 1784 (2001)
2 S.S. Mao, F. Quéré, S. Guizard, X. Mao, R.E. Russo, G. Petite, P. Martin: Appl. Phys. A: Mater. Sci. Process. **79**, 1695 (2004)
3 B.-T.V. Vu, O.L. Landen, A. Szoke: Phys. Plasmas **2**, 476 (1995)
4 X. Mao, S.S. Mao, R.E. Russo: Appl. Phys. Lett. **82**, 697 (2003)
5 D. von der Linde, H. Schüler: J. Opt. Soc. Am. B **13**, 216 (1996)
6 F. Quéré, S. Guizard, P. Martin, G. Petite, O. Gobert, P. Meynadier, M. Perdrix: Appl. Phys. B **68**, 459 (1999)
7 R. Lindner, M. Reichling, R.T. Williams, E. Matthias: J. Phys.: Condens. Matter **13**, 2339 (2001)
8 M. Li, S. Menon, J.P. Nibarger, G.N. Gibson: Phys. Rev. Lett. **82**, 2394 (1999)
9 G. Petite, S. Guizard, P. Martin, F. Quéré: Phys. Rev. Lett. **83**, 5182 (1999)
10 R. Stoian, M. Boyle, A. Thoss, A. Rosenfeld, G. Korn, I.V. Hertel: Appl. Phys. A: Mater. Sci. Process. **77**, 265 (2003)
11 P.R. Herman, A. Oettl, K.P. Chen, R.S. Marjoribanks: Proc. SPIE **3616**, 148 (1999)
12 I.H. Chowdhury, X. Xu, A.M. Weiner: Proc. SPIE **4978**, 138 (2003)
13 C. Ziener, P.S. Foster, E.J. Divall, C.J. Hooker, M.H.R. Hutchinson, A.J. Langley, D. Neely: J. Appl. Phys. **93**, 768 (2003)
14 G. Doumy, F. Quéré, O. Gobert, M. Perdrix, Ph. Martin, P. Audebert, J.C. Gauthier, J.-P. Geindre, T. Wittmann: Phys. Rev. E **69**, 26402 (2004)
15 M. Mlejnek, E.M. Wright, J.V. Moloney: Opt. Lett. **23**, 382 (1998)
16 N.W. Ashcroft, N.D. Mermin: *Solid State Physics* (Holt, Rinehart and Winston, New York 1976)
17 Z.A. Weinberg, G.W. Rubloff, E. Bassous: Phys. Rev. B **19**, 3107 (1979)
18 D.G. Hicks, P.M. Celliers, G.W. Collins, J.H. Eggert, S.J. Moon: Phys. Rev. Lett. **91**, 35502 (2003)
19 L.V. Keldysh: Sov. Phys. JETP **20**, 1307 (1965)
20 Q. Wu, I.H. Chowdhury, X. Xu: Phys. Rev. B, in press
21 D.R. Lide, H.V. Kehiaian: *CRC Handbook of Thermophysical and Thermochemical Data* (CRC, Boca Raton, FL 1994)
22 I.H. Chowdhury, X. Xu, A.M. Weiner: Appl. Phys. Lett. **86**, 151110 (2005)
23 V. Koubassov, J.F. Laprise, F. Théberge, E. Förster, R. Sauerbrey, B. Müller, U. Glatzel, S.L. Chin: Appl. Phys. A: Mater. Sci. Process. **79**, 499 (2004)
24 S. Krishnan, J.K.R. Weber, R.A. Schiffman, P.C. Nordine: J. Am. Ceram. Soc. **74**, 881 (1991)
25 J.K.R. Weber, S. Krishnan, C.D. Anderson, P.C. Nordine: J. Am. Ceram. Soc. **78**, 583 (1995)
26 A. Rosenfeld, D. Ashkenasi, H. Varel, M. Wähmer, E.E.B. Campbell: Appl. Surf. Sci. **127**, 76 (1998)